Naval Research Laboratory
Washington, DC 20375-5320

NRL/MR/5650--05-8904

Design and Characterization of Long-Haul Single-Channel Intensity-Modulated Analog Fiber-Optic Links

VINCENT J. URICK
LEE SWINGEN
MATTHEW S. ROGGE
ANTHONY L. CAMPILLO
FRANK BUCHOLTZ
JAMES L. DEXTER

Photonics Technology Branch
Optical Sciences Division

PATRICK F. KNAPP

SFA, Inc.
Crofton, Maryland

September 29, 2005

REPORT DOCUMENTATION PAGE

Form Approved
OMB No. 0704-0188

1. REPORT DATE *(DD-MM-YYYY)*	2. REPORT TYPE	3. DATES COVERED *(From - To)*
29-09-2005	Memorandum	March 23, 2005 - July 14, 2005

4. TITLE AND SUBTITLE

Design and Characterization of Long-Haul Single-Channel Intensity-Modulated Analog Fiber-Optic Links

5a. CONTRACT NUMBER

5b. GRANT NUMBER

5c. PROGRAM ELEMENT NUMBER

6. AUTHOR(S)

Vincent J. Urick, Patrick F. Knapp,* Lee Swingen, Matthew S. Rogge, Anthony L. Campillo, Frank Bucholtz, and James L. Dexter

5d. PROJECT NUMBER

5e. TASK NUMBER

5f. WORK UNIT NUMBER

7. PERFORMING ORGANIZATION NAME(S) AND ADDRESS(ES)

Naval Research Laboratory
4555 Overlook Ave., SW
Washington, DC 20375

*SFA, Inc.
2200 Defense Highway, Suite 405
Crofton, MD 21114

8. PERFORMING ORGANIZATION REPORT NUMBER

NRL/MR/5650--05-8904

9. SPONSORING / MONITORING AGENCY NAME(S) AND ADDRESS(ES)

Office of Naval Research
800 North Quincy Street
Arlington, VA 22217

10. SPONSOR / MONITOR'S ACRONYM(S)

ONR

11. SPONSOR / MONITOR'S REPORT NUMBER(S)

12. DISTRIBUTION / AVAILABILITY STATEMENT

Approved for public release; distribution is unlimited.

13. SUPPLEMENTARY NOTES

14. ABSTRACT

We present a self-contained guide for the design and characterization of long-haul single-channel intensity-modulated analog fiber-optic links. A high-performance 20 km fiber delay line is used to demonstrate the design considerations that are developed.

15. SUBJECT TERMS

Long-haul fiber-optic link; Analog photonics; Fiber amplifiers; Spurious-free dynamic range

16. SECURITY CLASSIFICATION OF:			17. LIMITATION OF ABSTRACT	18. NUMBER OF PAGES	19a. NAME OF RESPONSIBLE PERSON
a. REPORT	b. ABSTRACT	c. THIS PAGE			Vincent J. Urick
Unclassified	Unclassified	Unclassified	UL	23	19b. TELEPHONE NUMBER *(include area code)* (202) 767-9352

TABLE OF CONTENTS

DESIGN AND CHARACTERIZATION OF LONG-HAUL SINGLE-CHANNEL INTENSITY-MODULATED ANALOG FIBER-OPTIC LINKS

EXECUTIVE SUMMARY

- This report provides a complete guide to the design, characterization, and analysis of single-channel long-haul analog fiber-optic links.
- Important applications of long-haul analog links include antenna remoting, true time delay lines, and optoelectronic oscillators.
- Outlined here are the design considerations and procedures for building a high-performance long-haul analog link.
- Included in this report are the theoretical equations for radio frequency noise figure, gain, and spurious-free dynamic range in the signal-spontaneous beat noise limit.
- An experimental verification of the equations is provided and a 20 km high-performance link is characterized and demonstrated.

Manuscript approved August 2, 2005.

DESIGN AND CHARACTERIZATION OF LONG-HAUL SINGLE-CHANNEL INTENSITY-MODULATED ANALOG FIBER-OPTIC LINKS

1 INTRODUCTION

High-performance analog fiber optic links with lengths greater than a few kilometers are required for many military applications. Examples of such needs include, but are not limited to, antenna remoting, delay lines for signal processing, wideband analog networks, and optoelectronic oscillators. Such links require higher spurious-free dynamic range (SFDR) and instantaneous bandwidth than typical commercial systems. Previously, we have demonstrated high-performance hybrid fiber-optic links, capable of supporting analog and digital modulation formats [1],[2], the results of which have significant bearing on future military systems. Here, we present a stand-alone guide for the design and characterization of such long-haul analog fiber-optic links. For simplicity, we restrict the discussion to single-channel intensity-modulated links, noting that research is presently being carried out on long-haul multi-channel analog links [3]-[6] and novel analog modulation formats for long-haul transmission [7]-[10].

This report assumes limited knowledge of analog photonics with Section 2 describing a general analog photonic link in terms of gain and typical sources of noise. Section 3 addresses the impairments imposed by long-haul transmission through fiber, namely chromatic dispersion, stimulated Brillouin scattering, and optical amplifier noise. The most inclusive metric for analog links, SFDR, is theoretically described in Section 4 where the design issues for a long-haul analog link are summarized. Section 5 then demonstrates the methodology of designing a long-haul analog link, including the measurement of the parameters discussed in previous sections. Finally, the work is summarized and put into perspective in Section 6.

2 THE TRADITIONAL PHOTONIC LINK

2.1 External Modulation and Direct Detection

Though many techniques have been proposed for analog fiber-optic transmission, we define an externally-modulated link employing direct detection as the general photonic link. A generic schematic of such a link is shown in Fig. 1, where a laser is externally modulated by an RF voltage V_{rf} using a Mach-Zehnder modulator (MZM) biased by a DC voltage V_b. The resulting intensity-modulated optical carrier then traverses some fiber length and is detected using a p-i-n photodiode. An uncompressed photodiode responds linearly to the incident photon intensity, resulting in an RF photocurrent I_{rf} from which the modulation signal is recovered.

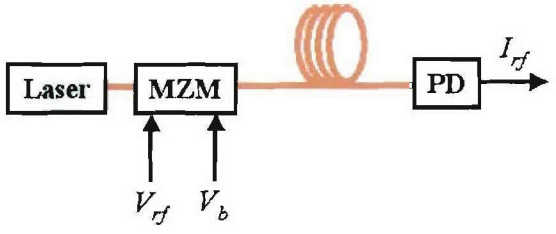

Fig. 1. Diagram of a traditional photonic link showing a laser, Mach-Zehnder modulator (MZM) and photodiode (PD). V_{rf}: applied signal voltage, V_b: DC bias voltage, I_{rf}: RF photocurrent.

The link in Fig. 1 may be described mathematically by first writing the optical field entering the MZM as $E(t)=q\sqrt{2P_o}e^{i\omega_o t}$ where $\omega_o/2\pi$ is the center frequency of the laser, P_o is the laser power, and q is a constant relating optical electric field and power. The drive voltage is written as $V_{drive}=V_b+V_{rf}\sin\Omega t$ where V_b is the DC bias voltage and V_{rf} is the signal voltage at frequency $f=\Omega/2\pi$. Assuming a push-pull (balanced) MZM, this drive produces a phase shift in each arm of the MZM given by $\phi(t)/2=\phi_b/2+(\phi_0/2)\sin\Omega t$. Here, $\phi_b\equiv\pi V_b/V_\pi$ is the phase change due to the bias and $\phi_0\equiv\pi V_{rf}/V_\pi$, where V_π is the peak voltage required to produce π peak phase shift, a frequency-dependent characteristic of the MZM. Assuming no loss, the electric fields at the two outputs of the MZM are calculated using

$$\begin{bmatrix}E_{out1}(t)\\E_{out2}(t)\end{bmatrix}=\frac{1}{\sqrt{2}}\begin{bmatrix}1 & i\\ i & 1\end{bmatrix}\begin{bmatrix}e^{i\phi(t)/2} & 0\\ 0 & e^{-i\phi(t)/2}\end{bmatrix}\frac{1}{\sqrt{2}}\begin{bmatrix}1 & i\\ i & 1\end{bmatrix}\begin{bmatrix}E(t)\\0\end{bmatrix} \tag{1}$$

which gives the two MZM outputs as

$$\begin{bmatrix}E_{out1}(t)\\E_{out2}(t)\end{bmatrix}=\frac{q\sqrt{2P_o}}{2}\begin{bmatrix}e^{i(\omega_o t+\phi(t)/2)}-e^{i(\omega_o t-\phi(t)/2)}\\ ie^{i(\omega_o t+\phi(t)/2)}+ie^{i(\omega_o t-\phi(t)/2)}\end{bmatrix} \tag{2}$$

Arbitrarily choosing $E_{out1}(t)$ as the field that is detected, we calculate the optical power incident on the photodetector using the convention $P_{opt}=|E_{out1}(t)|^2/2q^2$ as

$$P_{opt}=\frac{P_o}{4}\left(2-e^{i\phi(t)}-e^{-i\phi(t)}\right)=\frac{P_o}{4}\left(2-2\cos\phi(t)\right)=\frac{I_t}{\Re} \tag{3}$$

where I_t is the total photocurrent and $\Re$ is the detector responsivity. To expand (3), we set $\phi_b=\pi/2$ (quadrature bias) and use the identity $\sin(x\sin\theta)=2\sum_{n=0}^{\infty}J_{2n+1}(x)\sin[(2n+1)\theta]$, arriving at

$$I_t=\Re P_o\left(\frac{1}{2}+\sum_{n=0}^{\infty}J_{2n+1}(\phi_0)\sin[(2n+1)\Omega t]\right) \tag{4}$$

where J_m are m^{th} order Bessel functions of the first kind. Note that (4) contains a DC term, $I_{dc}=\Re P_o/2$, and RF terms at the fundamental frequency $\Omega/2\pi$ and its odd harmonics, $I_{rf}=\Re P_o\sum_{n=0}^{\infty}J_{2n+1}(\phi_0)\sin[(2n+1)\Omega t]\equiv\sum_{n=0}^{\infty}I((2n+1)\Omega t)\sin[(2n+1)\Omega t]$. It is important to point out that (4) is exact only for an ideal MZM with no insertion loss.

Before calculating the RF power delivered by the link, it is important to discuss the detector circuit. Many techniques are employed for the packaging of photodiodes such that they deliver maximum RF frequency and power performance. For this analysis, we assume an internal impedance-matching circuit associated with the detector, as shown in Fig. 2. This type of packaging typically increases the bandwidth of the detector but limits its RF power output. For this impedance-matched system, only half of the generated I_{rf} is delivered to the AC-coupled

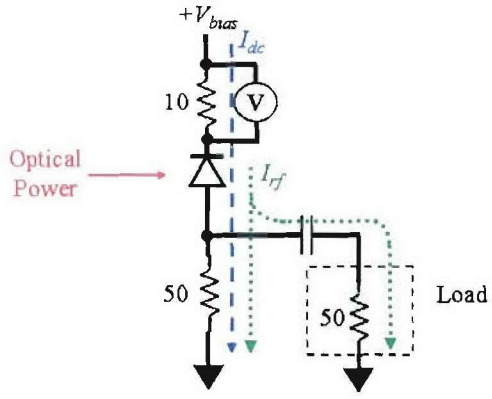

Fig. 2. Circuit diagram for a photodetector impedance matched to an AC-coupled load. The DC current follows the dashed blue path while the RF current follows the dotted green path. The DC current is measured through a series 10 Ω resistor.

load, as shown by the dotted green path in Fig. 2, while all of the DC photocurrent (dashed blue path) is measured using, for example, a series resistor as shown. The I_{dc} and I_{rf} used for the remainder of this report will, in all cases, assume the circuit in Fig. 2.

From (4) we then have for the delivered RF fundamental power

$$P_{out} = \frac{1}{2}\left(\frac{I(\Omega)}{2}\right)^2 Z = \frac{1}{8}\left[\Re P_0 J_1(\phi_0)\right]^2 Z = \frac{1}{2} I_{dc}^2 J_1^2(\phi_0) Z \tag{5}$$

(Again the factor of 1/2 in I(Ω)/2 results from the circuit in Fig. 2.) If we now require that $V_{rf} << V_\pi$ ($\phi_0 << 1$), we can use the approximation $J_1(\phi_0) \approx \phi_0/2$ and rewrite (5) as

$$P_{out} = \frac{1}{8} I_{dc}^2 Z \left(\frac{\pi V_{rf}}{V_\pi}\right)^2 \tag{6}$$

Recalling that V_{rf} is the input drive voltage and assuming impedance matching, we can insert $V_{rf}^2 = 2P_{in}Z$ into (6) which gives an expression for the RF gain as

$$g_{rf} = \frac{P_{out}}{P_{in}} = \left(\frac{I_{dc}}{V_\pi}\right)^2 \frac{\pi^2 Z^2}{4} \tag{7}$$

Using $Z = 50\ \Omega$, the dB version of the link gain is then given by

$$G_{rf}[\text{dB}] = -22 - 20\log(V_\pi[\text{V}]) + 20\log(I_{dc}[\text{mA}]) \tag{8}$$

This result (8) is very important and will be used throughout the remainder of this report. It serves as a design rule for maximizing RF gain: use the lowest V_π modulator available and maximize the photocurrent. Note that (8) assumes 1) I_{dc} corresponds only to light that has passed through the modulator and 2) the circuit in Fig. 2 is employed.

2.2 Noise in a Photonic Link

Neglecting for now the noise introduced by optical amplification and fiber nonlinearites, there are four noise sources in a single-channel photonic link: input thermal noise, output thermal noise, detector shot noise, and laser relative intensity noise (RIN). Here, we treat each noise source briefly and refer the reader to citations for a more detailed discussion.

Thermal or Johnson noise [11] is a white noise associated with any resistor in thermal equilibrium. For matched resistors in thermal equilibrium at temperature T, the delivered thermal noise power spectral density is given by $N_{th} = k_B T$, where $k_B = 1.381 \times 10^{-23}$ J/K is Boltzmann's constant. For T = 300 K, N_{th} = -174 dBm/Hz. Noting that the input thermal noise experiences the link gain (8) we have for the input and output thermal noise power spectral densities

$$\begin{aligned} N_{ith}[\text{dBm/Hz}] &= -174 - 22 - 20\log(V_\pi[\text{V}]) + 20\log(I_{dc}[\text{mA}]) \\ N_{oth}[\text{dBm/Hz}] &= -174 \end{aligned} \tag{9}$$

Detector shot noise [12], like thermal noise, is white. On the most basic level, shot noise arises due to the quantization of the electric field. The rms current spectral density for shot noise is given by $i_{sh}\left[\text{A}/\sqrt{\text{Hz}}\right] = \sqrt{2eI}$ where $e = 1.602 \times 10^{-19}$ C and I is the DC photocurrent. For the system discussed here (Fig. 2), the RMS RF photocurrent at the load resistor due to shot noise is $\sqrt{2eI}/2$ and the shot noise power spectral density is given by

$$N_{sh}[\text{dBm/Hz}] = 10\log\left(\frac{eZI_{dc}[\text{mA}]}{2}\right) = -174 + 10\log(I_{dc}[\text{mA}]) \tag{10}$$

Laser RIN, on the other hand, is certainly not spectrally white. It is a function of frequency separation from the optical carrier and typically has a strong peak at the relaxation frequency of the laser. RIN is due to many statistical processes associated with a laser cavity such as amplified spontaneous emission and side modes. Here we mean laser RIN to include any intensity noise that the laser adds to the system, whatever the cause may be. Laser RIN is typically defined as [13] $rin \equiv \langle \Delta P^2 \rangle / \langle P \rangle^2$ where $\langle \Delta P^2 \rangle$ is the mean square intensity fluctuation spectral density and $\langle P \rangle^2$ is the average laser power. RIN is specified in dBc/Hz, a measured quantity specific to each laser that is a function of frequency. The RIN power spectral density for our system is then

$$N_{laser}[\text{dBm/Hz}] = -19 + 20\log(I_{dc}[\text{mA}]) + RIN[\text{dBc/Hz}] \tag{11}$$

We can now write expressions for total link noise N_t and RF noise figure NF_{rf} using (8)-(11). The total link noise is simply given by the linear sum of (9)-(11) from which the noise figure is calculated as

$$NF_{rf}[\text{dB}] \equiv SNR_{in}[\text{dB}] - SNR_{out}[\text{dB}] = 174 - G_{rf}[\text{dB}] + N_t[\text{dBm/Hz}] \tag{12}$$

where a thermally-limited input is assumed. These results are plotted in Figs. 3 and 4. Fig. 3 shows the noise floor for a photonic link as a function of I_{dc} for V_π = 2.12 V and RIN = -165 and -200 dBc/Hz. The limiting noise sources are also shown in Fig. 3. Note that RIN = -165 dBc/Hz will ultimately limit the link performance (Fig. 3a) whereas for RIN = -200 dBc/Hz input thermal

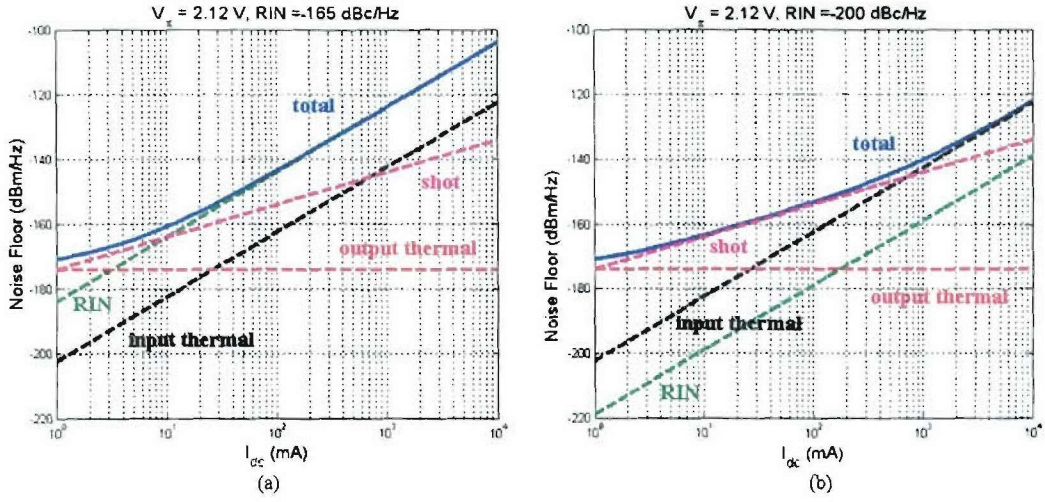

Fig. 3. Link noise floor as a function of photocurrent for (a) RIN = -165 and (b) RIN = -200 dBc/Hz with V_π = 2.12 V. The total noise is shown in solid blue and the individual noise floors by dashed lines as follows: shot noise (pink), output thermal noise (red), input thermal noise (black), and RIN (green).

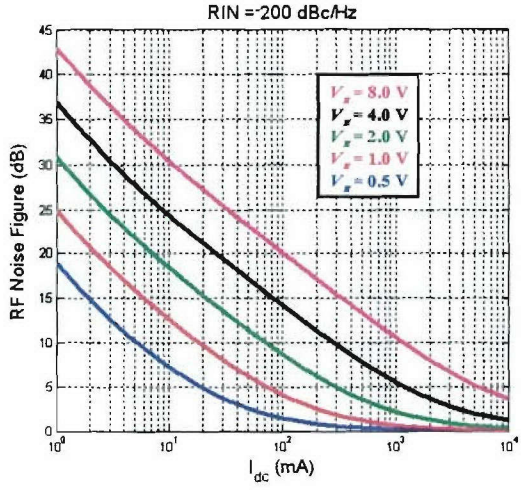

Fig. 4. RF noise figure as a function of photocurrent for five different V_π with RIN = -200 dBc/Hz.

noise will be the limit (Fig. 3b). For a low enough RIN, the total noise floor will shift from approximately shot-noise limited to input thermal-noise-limited at a photocurrent that depends on V_π. For higher V_π, this current increases. Fig. 4 shows NF_{rf} as a function of I_{dc} for different V_π depicting the trend that at low I_{dc} a lower NF_{rf} is achievable with lower V_π. However, they all converge to NF_{rf} = 0, albeit at presently unachievable photocurrents.

At this point, the design of a photonic link may seem trivial, namely, use a low-RIN high-power laser to maximize the delivered power to a detector that can handle high I_{dc}. This along with a low V_π modulator will maximize the performance of the photonic link. This is essentially the goal of a short link, where the system design reduces to component design. As will be discussed in the next section, this approach is not applicable for long-haul link design, where other limiting factors must be considered.

3 LONG-HAUL LINK IMPAIRMENTS

Transmitting a single analog signal over long distances of fiber is non-trivial, due primarily to the nonlinear nature of the fiber. This makes the system design more difficult in that there are limitations imposed by the link itself. In other words, if perfect transmit and receive components were available, the fiber itself will limit the analog performance of the link. Here, we treat the most important fiber impairments in single channel systems: chromatic dispersion, stimulated Brillouin scattering, and link loss. The latter may seem trivial but actually leads to the necessity of optical amplification, which in turn adds noise to the system.

3.1 Chromatic Dispersion in Analog Links

Chromatic dispersion in fiber is due to photon-electron interactions in the fiber that give rise to a frequency-dependent index of refraction and hence a frequency-dependent phase shift. Mathematically, this is described by writing the mode propagation constant explicitly in the electric field from which the RF power response can be derived.

The electric field for the output of an MZM as given by (2) treated only the temporal dependence of the field, an approach that was completely adequate for the discussion in Section 2. However, to describe chromatic dispersion and its impairments in long analog links, we must write the spatial dependence of the field as well. The field given by (2) can therefore be written in an expanded and more instructive form, including the spatial dependence as [10]

$$E_{out1}(z,t) = q\sqrt{P_o}J_0(\phi_0/2)\sin\left(\omega_o t - \beta_{\omega_o} z\right) + q\sqrt{P_o}\sum_{\substack{n=-\infty \\ n\neq 0}}^{\infty} J_n(\phi_0/2)\cos\left[(\omega_0 + n\Omega)t - \beta_{\omega_o + n\Omega} z\right] \quad (13)$$

where β_ν is the propagation constant at optical angular frequency ν. The form of (13) is instructive in that it describes how there is a comb of optical frequencies spread about the optical carrier spaced at the RF modulation frequency. The mode propagation constant $\beta(\nu)$ can then be expanded in a Taylor series about the optical carrier frequency ω_o as [14]

$$\beta(\nu) = \beta_o + \beta_1(\nu - \omega_o) + \frac{1}{2}\beta_2(\nu - \omega_o)^2 \quad (14)$$

where higher-order dispersion terms have been excluded and the coefficients in the expansion are given by [15] as $\beta_m = \left(d^m\beta/d\nu^m\right)_{\nu=\omega_o}$. The group velocity is given by $v_g = 1/\beta_1$ and the chromatic dispersion parameter of the fiber is $D = -2\pi c\beta_2/\lambda^2$ where c is velocity of light in vacuum and λ is the optical carrier frequency. Using these relations and inserting (14) into (13) the following expression can be obtained for the RF power at the fundamental frequency

$$P_{rf,out}(f) = \frac{1}{8}I_{dc}^2 Z\left(\frac{\pi V_{rf}}{V_\pi}\right)^2 \cos^2\left(\frac{\pi D\lambda^2 L f^2}{c}\right) \quad (15)$$

where L is the propagation length and small RF drive ($\phi_0 << 1$) is assumed. Note that for $D = 0$ the power for the fundamental (15) agrees with (6). However, for $D \neq 0$ (15) details how power penalties and extinctions can occur at the fundamental frequency.

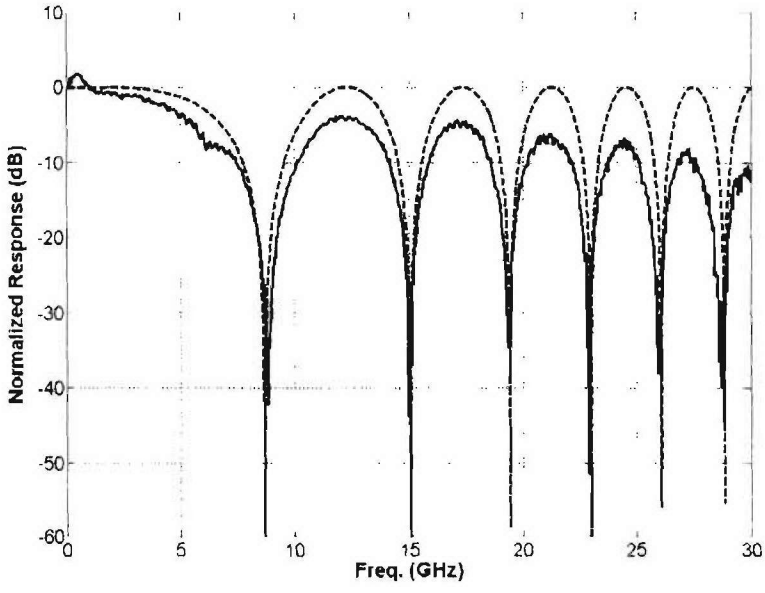

Fig. 5. Measured (solid) and calculated (dashed) dispersion response for an analog link through 50 km of SMF-28 fiber.

Fig. 5 shows the calculated and measured dispersion response for D = 17 ps/nm/km (standard SMF-28 fiber), λ = 1551 nm, and L = 50 km (the additional power penalty in the measured data is due to the MZM and detector frequency response). Note that for 50 km transmission, SMF-28 is inadequate for systems above a few GHz. It is important to note that for small modulation, all odd-order harmonics and intermodulation terms have a $\cos^2\left(\pi D\lambda^2 L f^2/c\right)$ frequency dependence while those of even order follow a $\sin^2\left(\pi D\lambda^2 L f^2/c\right)$ trend. Consequently, for frequencies at which the fundamental is relatively unaffected by dispersion, there may be a large increase in the level of even-order harmonics and intermodulation products, which can result in reduced SFDR [3],[16]. Considering all of this, it is desirable to have as low a net dispersion ($D \times L$) as possible when building a wideband analog link. As will be demonstrated, this may be accomplished by building the link with equal lengths of fibers having opposite and equal dispersion.

3.2 Stimulated Brillouin Scattering

Unlike the photon-electron interactions that cause chromatic dispersion in fiber, stimulated Brillouin scattering (SBS) is due to photon-phonon scattering. Phonons and solid lattice vibrations are analogous to photons and electromagnetic radiation in that phonons are the quanta of the energy in solid lattice vibrations [17]. Brillouin scattering is a nonelastic scattering where a photon loses energy to the crystal lattice. That is, a phonon can absorb some of the scattered photon energy, resulting in a frequency downshift of the scattered light. This scattered wave is often referred to as the Stokes wave and, due to conservation of momentum, propagates in the opposite direction of the incident light for the case of a telecommunication fiber. Furthermore, this entire process can be stimulated when the incident light has a high enough intensity and can be thought of as a resonant phenomenon. To understand the adverse effects that SBS can have on a long-haul fiber link, Rayleigh backscattering must also be considered. Rayleigh backscattering

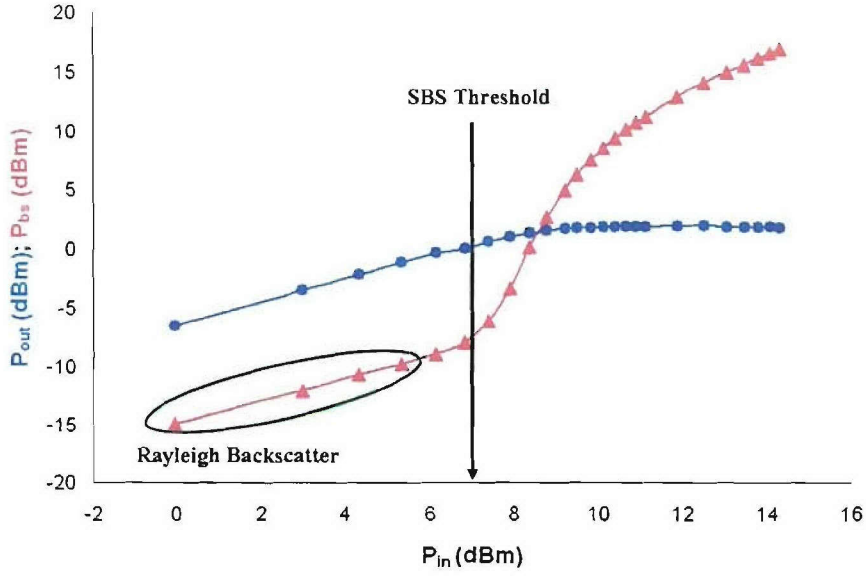

Fig. 6. Optical transmission curve for 20 km of SMF-28 using a 1551 nm DFB semiconductor laser as the probe. The output power as a function of input power is shown in blue circles and the backscattered power in red triangles.

is an elastic scattering which is typically linear. This qualitative description of the two scattering processes are all that is required to understand the detrimental effects of SBS in an analog link.
In long-haul analog links, SBS is troublesome for two reasons. First, signal photons that are meant to propagate the fiber to the receiver are scattered backward nonlinearly. In this sense, SBS limits the amount of power that can be transmitted through the fiber. Second, the SBS process adds noise to an analog system. For low input powers into a fiber, the input and output power are linearly related by some loss coefficient, which is typically dominated by Rayleigh scattering in the fiber. However, as the power is increased, this relationship becomes nonlinear due to SBS. In fact, SBS can completely saturate the output power of the fiber. Because SBS is a stimulated process there is a threshold associated with it, which can be written as [15]

$$P_{th} \approx \frac{21 A_{eff}}{g_B L_{eff}} \tag{16}$$

where A_{eff} is the effective area of the fiber, L_{eff} the effective length of the fiber, and g_B the peak value of the Brillouin gain. Therefore, as does the frequency shift associated with SBS, the SBS threshold depends on the fiber characteristics. It is also of note that 1) as the linewidth of the signal laser increases, P_{th} also increases and 2) for a particular fiber type, the SBS frequency is wavelength dependent. It is perhaps more instructive to analyze some measured data pertaining to SBS. Fig. 6 shows the measured optical power at the input and output of a 20 km link comprised of standard single mode fiber (SMF-28) using a 1551 nm DFB semiconductor laser as the probe. For input powers below 6 dBm, the output and backscattered power are linearly related to the input power. At about 7 dBm input power, the SBS threshold is achieved and the backscattered power increases rapidly, while the output power saturates. Just as the forward propagating wave experiences Rayleigh backscattering, the backward-propagating SBS wave Rayleigh backscatters to copropagate with the signal. When the SBS intensity is high enough its Rayleigh scattered counterpart beats with the signal wave, generating a spectrum at the output

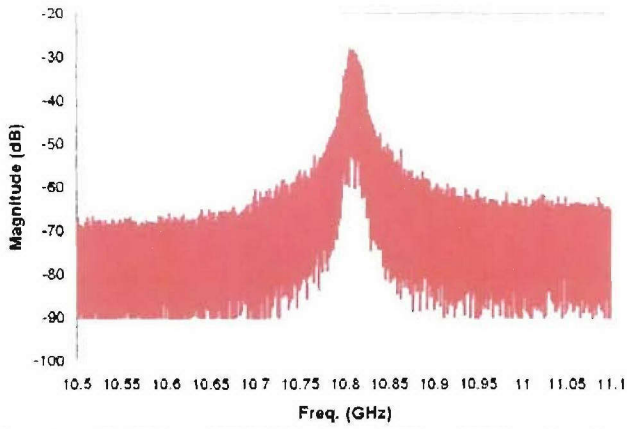

Fig. 7. Measured SBS spectrum for 20 km of SMF-28 using a 1551 nm DFB semiconductor laser as the probe.

centered at their separation frequency (i.e. the SBS frequency). This spectrum in the electrical domain is a convolution of the laser linewidth with the net phonon spectrum for the fiber. The spectrum for 20 km of SMF-28 is shown in Fig. 7 using a 1551 nm DFB semiconductor laser as the probe. From Fig. 7, the SBS frequency for SMF-28 is approximately 10.82 GHz. It must also be noted that the RF noise due to SBS is not limited to the SBS frequency. Rather, SBS can cause an increase in overall system phase and amplitude noise [18]. There are ways to combat SBS in analog links and we now turn to those.

There are many ways to increase the SBS threshold such that more power can be injected into a long-haul fiber optic link. These techniques include using sources with broader linewidths, dithering the transmitter [19], straining the transmission fiber [20], and applying a temperature gradient to the fiber [21]. A more passive technique that has been employed [1],[2] and thoroughly analyzed [22]-[25] is to construct the link from fibers that have different SBS frequencies. Because SBS is a distributed effect, alternating the fiber in short lengths of fibers with different SBS frequencies can serve to decouple the stimulated resonance and therefore increase the SBS threshold. This technique will be revisited and demonstrated in Section 5.

3.3 Optical Amplifier Noise

For long-haul analog transmission, some sort of optical amplification must be employed to compensate for the loss in the fiber. Erbium-doped fiber amplifiers (EDFA) are typically the amplifier of choice, given the mature technology and proven performance [26],[27]. Just as in the case of an RF amplifier, the optical gain for a cascade of EDFAs, G_{opt}, comes at the cost of a noise penalty, typically described by the cascaded EDFA noise figure NF_{opt}. This noise figure is defined relative to a shot-noise-limited SNR at the input to the EDFA as

$$NF_{opt}(\mathrm{dB}) \equiv SNR_{in} - SNR_{out} = RIN_{out} - RIN_{shot}^{in} \tag{17}$$

where RIN_{out} here is meant to describe the total RIN at the final EDFA output and RIN_{shot}^{in} is the RIN due to shot noise at the first EDFA input if a perfect (unity quantum efficiency) photodetector was used. This noise figure, and the noise power associated with the optical amplification process, can dominate over the other possible sources of noise described earlier in Section 2. However, a large SNR can be realized at the output by employing a highly-compressed EDFA. Fig. 8 shows G_{opt}, RIN_{out}, RIN_{shot}^{in} and NF_{opt} as a function of input power for a

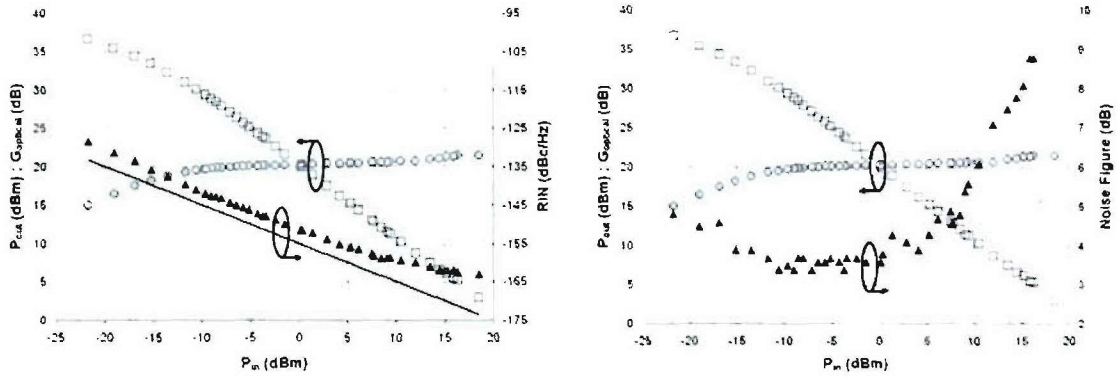

Fig. 8 (a) Optical gain (squares), optical output power (circles), output RIN (triangles) and input shot-noise-limited RIN (solid line) as a function of input power to a typical EDFA. (b) Calculated noise figure (triangles) for the same EDFA as a function of input power.

commercial EDFA, measured using a laser with -189 dBc/Hz RIN. Given the gain and noise figure, the electrical noise generated by signal-spontaneous beating can be calculated as [1]

$$N_{sig-sp}[\text{dBm/Hz}] = -175 + 10\log(\Re I'_{dc}[\text{mA}]) + G_{opt}[\text{dB}] + NF_{opt}[\text{dB}] \tag{18}$$

where $\Re$ is again the detector responsivity, $I'_{dc} = l_{opt} g_{opt} I_{dc} = \Re l_{opt} g_{opt} P_o/2$ with l_{opt} being the optical loss before the first amplifier, and the circuit in Fig. 2 is assumed (Note that the equations in Section 2 were derived for a link with no optical loss or gain; without loss of generality, the equations can be corrected for a link with optical gain by simply replacing I_{dc} with I'_{dc}). For an EDFA that is compressed, the signal-spontaneous beat noise (18) will dominate over the spontaneous-spontaneous beat noise. If however, the amplifier is uncompressed, an optical filter is typically employed to filter the amplified spontaneous emission such that the dominant noise term is given by (18). For completeness we derive the expression for spontaneous-spontaneous beat noise with an optical bandwidth B_o using the equations in [28] as

$$N_{sp-sp}[\text{dBm/Hz}] = -247 + 20\log(\Re) + 2G_{opt}[\text{dB}] + 2NF_{opt}[\text{dB}] + 10\log(B_o[\text{GHz}]) \tag{19}$$

Note that in Fig. 8, the noise figure rises at the lower input powers owing to the fact that spontaneous-spontaneous noise was not filtered for these data and increases the noise figure. Therefore, characteristics of the type shown in Fig. 8 must be considered when using EDFA(s) in a long-haul analog link, again noting that the noise generated in the amplification process will typically dominate all other sources of noise (12) at the output.

4 SPURIOUS-FREE DYNAMIC RANGE

The remaining link characteristic to consider is its linearity, as captured by the metric spurious-free dynamic range (SFDR). The SFDR in general is given by

$$SFDR\left[\mathrm{dB}\cdot\mathrm{Hz}^{(n-1)/n}\right]=\frac{(n-1)}{n}\left(OIPn[\mathrm{dBm}]-N_{out}[\mathrm{dBm/Hz}]\right) \tag{20}$$

where $OIPn$ is the output-referenced intercept point of the dominant n^{th}-order nonlinear term for a system and N_{out} is the total output noise. For a single-octave system, the two-tone third order intermodulation term dominates [29] and the output-referenced third-order intercept ($OIP3$) is used in (20). In general, a multi-octave system is limited by second order intermodulation. For a fiber-optic link employing an MZM biased at quadrature, the link linearity is limited by the linearity of the MZM and we will see that no second-order terms exist for an ideal MZM. Fig. 9 graphically shows the third-order limited SFDR for an MZM link.

To derive an analytical expression for an optically-amplified fiber-optic link with an MZM, we first redefine the SFDR as

$$SFDR\left[\mathrm{dB}\cdot\mathrm{Hz}^{2/3}\right]=\frac{2}{3}\left(OIP3[\mathrm{dBm}]-N_{sig-sp}[\mathrm{dBm/Hz}]\right) \tag{21}$$

where we have used the assumption that the dominant noise term is signal-spontaneous beat noise. (Note that the equations for link noise given in Section 2 can be used in the absence of optical amplification.) The remaining task is to derive an expression for the $OIP3$. To derive an analytical expression for $OIP3$, we first rewrite the total photocurrent (3) with quadrature bias ($\phi_b=\pi/2$) as $I_t=I_{dc}\left(1+\sin\phi'(t)\right)$. To evaluate the system linearity, we assume two sinusoidal drive voltages to the MZM, such that $\phi'(t)=\phi_1\sin\Omega_1 t+\phi_2\sin\Omega_2 t$ with $\phi_{1,2}=\pi V_{1,2}/V_\pi$ and $f_{1,2}=\Omega_{1,2}/2\pi$. This results in a total photocurrent given by $I_t=I_{dc}\left[1+\sin(\phi_1\sin\Omega_1 t+\phi_2\sin\Omega_2 t)\right]$. Using the same procedure in deriving (4) from (3), we arrive at an expression for the RF photocurrent:

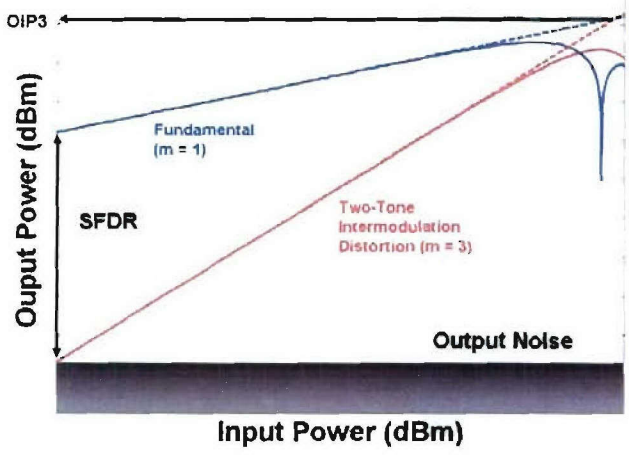

Fig. 9. Graphical representation of the spurious-free dynamic range for a fiber-optic link limited by the linearity of an MZM.

$$I_{rf,2\text{-}tone} = 2I_{dc}\left\{\begin{array}{l} J_0(\phi_2)\sum_{k=0}^{\infty} J_{2k+1}(\phi_1)\sin[(2k+1)\Omega_1 t] \pm \sum_{k=0}^{\infty}\sum_{m=1}^{\infty} J_{2k+1}(\phi_1)J_{2m}(\phi_2)\sin[(2m\Omega_2 \pm (2k+1)\Omega_1)t] \\ + J_0(\phi_1)\sum_{l=0}^{\infty} J_{2l+1}(\phi_2)\sin[(2l+1)\Omega_2 t] \pm \sum_{l=0}^{\infty}\sum_{n=1}^{\infty} J_{2l+1}(\phi_2)J_{2n}(\phi_1)\sin[(2n\Omega_1 \pm (2l+1)\Omega_2)t] \end{array}\right\} \tag{22}$$

Note that (22) contains only odd-order terms. If we assume that $V_1 = V_2 << V_\pi$ (with $|f_1 - f_2|$ small enough such that the frequency dependence of V_π can be neglected), then $\phi_1 = \phi_2 = \phi << 1$ and we can use the Bessel approximation $J_n(\phi) \approx \phi^n / (2^n n!)$. These approximations give the six largest terms of (22) as

$$\begin{array}{ll} I_{dc}\phi\sin(\Omega_{1,2}t) & (\text{fundamental}) \\ \pm\dfrac{I_{dc}\phi^3}{8}\sin[(2\Omega_{1,2} \pm \Omega_{2,1})t] & (\text{lowest-order intermodulation}) \end{array} \tag{23}$$

The *OIP*3 is defined as the output power at the intersection of these linear approximations, that is, where the fundamental level is equal to the level of the lowest-order distortion. The input voltage that yields the *OIP*3 is therefore given by the condition $I_{dc}\phi = I_{dc}\phi^3/8$, which results in $V_{OIP3} = 2\sqrt{2}V_\pi/\pi$. Inserting V_{OIP3} into the linear approximation for power in the fundamental (6) gives $OIP3 = I_{dc}^2 Z$, which can be written as (assuming $Z = 50\ \Omega$)

$$OIP3[\text{dBm}] = -13 + 20\log(I_{dc}[\text{mA}]) \tag{24}$$

Note that *OIP*3 is independent of V_π, depending only on the received photocurrent. Inserting (24) and (18) into (21) gives the desired expression for the SFDR of a long-haul link limited by signal-spontaneous beat noise as

$$SFDR[\text{dB}\cdot\text{Hz}^{2/3}] = \frac{2}{3}\{162 + 10\log(I'_{dc}[\text{mA}]) - G_{opt}[\text{dB}] - NF_{opt}[\text{dB}] - 10\log(\Re)\} \tag{25}$$

where I_{dc} was replaced with I'_{dc} in (24). We now have a complete set of equations for the design of a long-haul analog fiber-optic link. Equation (25) gives the design conditions for maximizing link linearity; (8) and (12), with $I'_{dc} = l_{opt}g_{opt}I_{dc} = \Re l_{opt}g_{opt}P_o/2$ and $N_{sig\text{-}sp}$ included in N_t, dictate the conditions for link gain and noise figure requirements. In addition, (15) and (16) detail the dominant fiber nonlinearities for a single-channel link. The remainder of this report is dedicated to demonstrating the use of these equations in the design of a 20 km analog delay line, which will also serve as a tutorial on measuring the parameters described in these preceding sections.

5 DESIGN AND CHARACTERIZATION OF A 20 KM LINK

Here we present the design and characterization of a 20 km long-haul analog fiber optic link. The link is intended to operate over the 10 MHz to 18 GHz frequency range. In addition, the link is required to have a SFDR greater than 100 $dB \cdot Hz^{2/3}$ and an RF loss less than 10 dB, both at 2 GHz. To meet the bandwidth requirements, a dispersion-managed fiber span must be used. For the loss and SFDR specifications, SBS management and an EDFA (with the tradeoffs between optical gain and optical noise figure taken into account) must be employed. Because specific link design considerations will vary on a case-by-case basis, we will simply show the architecture of a link and demonstrate that it does in fact meet the above specifications. After completing the analysis of this link, the issues associated with link design and the utility of the previously given equations should be evident.

The architecture of the 20 km link is shown in Fig. 10. The transmitter is a distributed feedback (DFB) semiconductor laser at 1551 nm with RIN < -165 dBc/Hz at 2 GHz. The MZM has a low V_π = 2.12 V at 2 GHz, which was chosen to maximize G_{rf} (8). As shown in Fig. 10, the fiber span was built from alternating sections of positive- and negative-dispersion fiber, with optical isolators placed mid span. This arrangement served to mitigate the adverse effects of chromatic dispersion on the frequency response. In addition, the two fiber types have different SBS frequencies. Therefore, the alternating arrangement along with the optical isolators serves to increase the SBS threshold. An EDFA was placed at the end of the link to compensate link loss and the p-i-n photodiode ($\Re = 0.8$ A/W) employs the RF circuit in Fig. 2. We will first characterize the fiber span and then follow with the RF link performance.

To ensure that chromatic dispersion does not affect the frequency response of the overall system, an expensive high-frequency MZM and photodetector pair were used in conjunction with a high-frequency network analyzer to measure the fiber frequency response. (The high-frequency MZM and photodetector were not employed in the final link design because of their cost, optical loss, and power handling capability). Fig. 11 shows the normalized RF frequency response with these components, showing the first dispersion null at about 46 GHz. From this value, the normalized fiber response can be calculated using (15) and is shown along with the measured response in Fig. 11. The calculation uses D = 1.45 ps/nm/km, λ = 1551 nm and L = 20 km, which gives a net dispersion of 29 ps/nm. Note that the fiber itself has no appreciable penalty up to

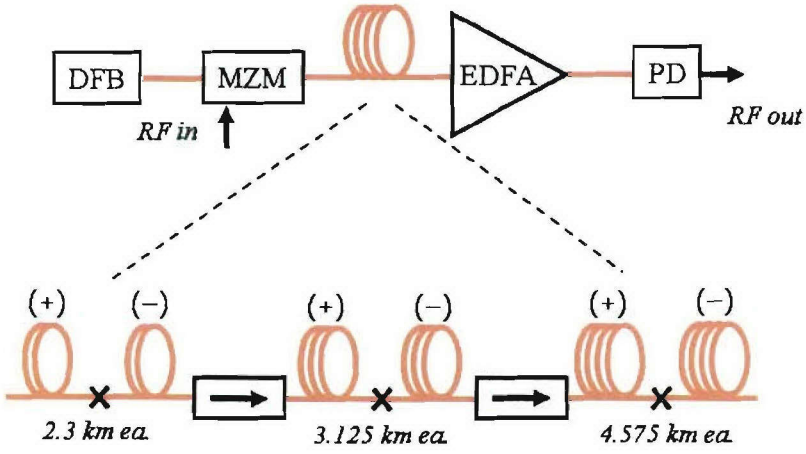

Fig. 10. Architecture for the 20 km link, showing the fiber arrangement. DFB: distributed feedback laser, MZM: Mach-Zehnder modulator, EFDA: Erbium-doped fiber amplifier, PD: photodetector, (+): positive-dispersion fiber, (-): negative-dispersion fiber, arrows: optical isolators.

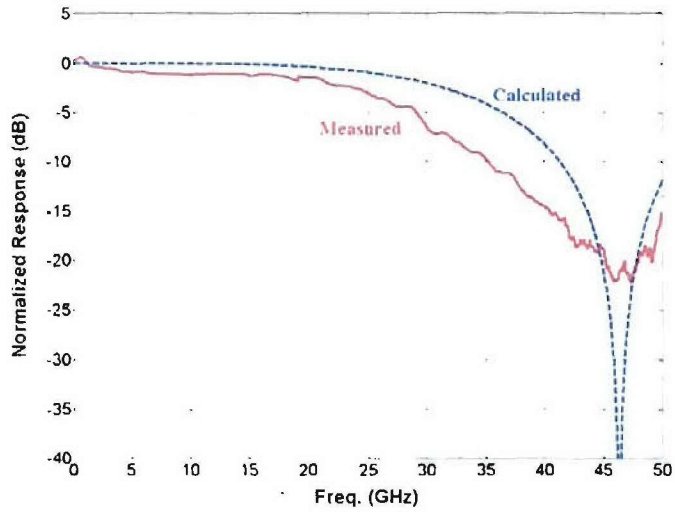

Fig. 11. Normalized frequency response for the fiber. Solid red: measured with high-frequency MZM and photodiode, dashed blue: calculated using location of first dispersion null.

18 GHz and has a 3-dB bandwidth greater than 30 GHz. For comparison, a 20 km span of SMF-28 has a net dispersion of 340 ps/nm, which yields the first dispersion null at about 13.5 GHz. In the case that the first dispersion null is too high in frequency to measure, the modulation phase shift method can be used to measure the chromatic dispersion [30]. To measure the optical power response for the fiber span, the optical output power and optical power scattered back to the link input were measured as a function of input power using optical power meters. The results of this measurement are shown in Fig. 12. From these data, an SBS threshold of 14 dBm can be specified. This will be more than adequate for the link in question and is 7 dB higher than the SBS threshold for 20 km of SMF-28 (see Fig. 6). For the last data point in Fig. 12, that is for about 18 dBm input power, the electrical spectrum after direct detection at the output of the link was measured and is shown in Fig. 13, where the differing SBS frequencies for the two fiber types are clear. While separated by only 40 MHz, the increase in SBS threshold compared to SMF-28, which has one SBS peak (see Fig. 7), remains significant.

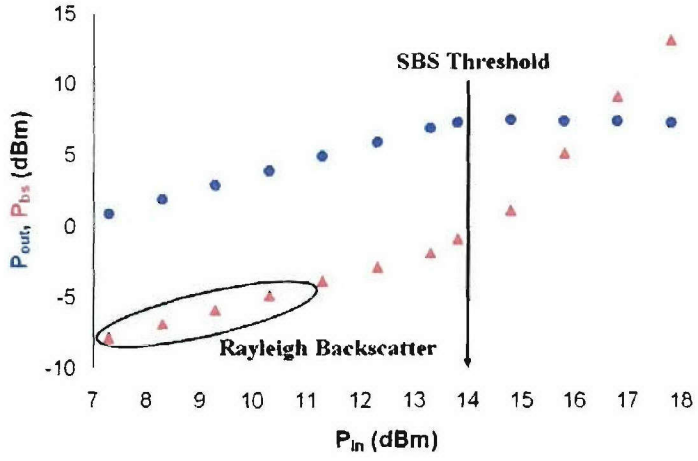

Fig. 12. The measured optical power response for the fiber span, showing output optical power (blue circles) and optical backscattered power (red triangles) as a function of input power.

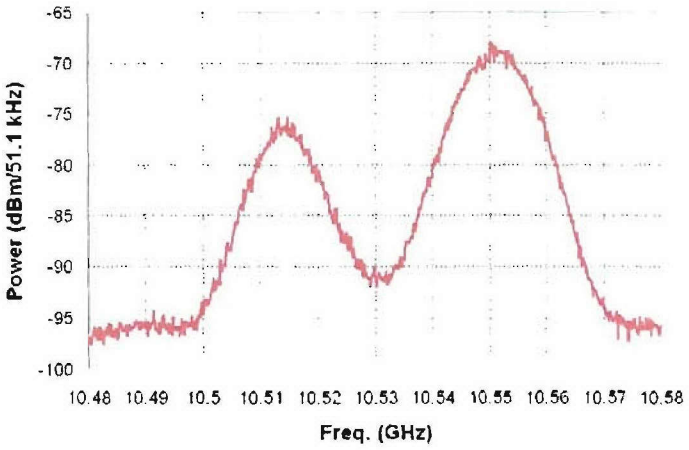

Fig. 13. Electrical direct-detection spectrum at the output of the 20 km fiber span with 18 dBm input power.

The fiber span can therefore support 17.5 GHz of RF bandwidth and handle up to about 13 dBm input power without adversely affecting the RF performance. To illustrate the RF design considerations for an optically-amplified link limited by signal-spontaneous beat noise (18), here we collect (8), (12), and (25).

$$G_{rf}[\mathrm{dB}] = -22 - 20\log(V_\pi[\mathrm{V}]) + 20\log(I'_{dc}[\mathrm{mA}]) \tag{26}$$

$$NF_{rf}[\mathrm{dB}] = 21 + 20\log(V_\pi[\mathrm{V}]) - 10\log(I'_{dc}[\mathrm{mA}]) + 10\log(\Re) + G_{opt}[\mathrm{dB}] + NF_{opt}[\mathrm{dB}] \tag{27}$$

$$SFDR\left[\mathrm{dB}\cdot\mathrm{Hz}^{2/3}\right] = \frac{2}{3}\left\{162 + 10\log(I'_{dc}[\mathrm{mA}]) - G_{opt}[\mathrm{dB}] - NF_{opt}[\mathrm{dB}] - 10\log(\Re)\right\} \tag{28}$$

where again $I'_{dc} = \Re l_{opt} g_{opt} P_o / 2$. Explicitly inserting I'_{dc} into the above equations can be more instructive:

$$G_{rf}[\mathrm{dB}] = -28 - 20\log(V_\pi[\mathrm{V}]) + 20\log(\Re) + 2P_o[\mathrm{dBm}] + 2G_{opt}[\mathrm{dB}] - 2L_{opt}[\mathrm{dB}] \tag{29}$$

$$NF_{rf}[\mathrm{dB}] = 24 + 20\log(V_\pi[\mathrm{V}]) - P_o[\mathrm{dBm}] + NF_{opt}[\mathrm{dB}] + L_{opt}[\mathrm{dB}] \tag{30}$$

$$SFDR\left[\mathrm{dB}\cdot\mathrm{Hz}^{2/3}\right] = \frac{2}{3}\left\{159 + P_o[\mathrm{dBm}] - NF_{opt}[\mathrm{dB}] - L_{opt}[\mathrm{dB}]\right\} \tag{31}$$

where $L_{opt}[\mathrm{dB}] = 10\log(1/l_{opt})$. (Also, recall that P_o is the optical input power into a lossless MZM). Equations (26)-(31) then explicitly detail the design tradeoffs in the signal-spontaneous limit. Obviously, V_π should be minimized noting that the loss of a real MZM must also be considered when designing a link. Another observation is that the launch power into the link and optical gain should be maximized, whereas the optical noise figure should be minimized. In reality, the design is not this simple in that P_o, G_{opt}, and NF_{opt} are not independent of each other. In practice, the amount of optical power available (depending on the laser power, MZM loss, and SBS threshold) must be considered along with the response(s) of the EDFA(s) in the link.

Making note of this, a weak generalization can be made as to the simultaneous optimization of (29)-(31): maximize P_o as long as it does not degrade NF_{opt}, while adjusting G_{opt} to achieve the desired G_{rf} as long as it does not degrade NF_{opt}. Many other such generalizations can be made, depending on which metric is to be optimized and which parameters are fixed.

Because $V_\pi = 2.12$ V at 2 GHz is minimized for this 20 km link, we set the launch power after the MZM at 11.9 dBm (just below the SBS threshold) and adjusted the gain of the EDFA to achieve the specified link loss at 2 GHz. The resulting G_{opt} was 7 dB, which gave $I'_{dc} = 13$ mA. As shown in Fig. 14, the RF frequency response measured on a network analyzer, this resulted in an RF loss of 9.5 dB at 2 GHz (G_{rf} = -9.5 dB). Checking these values against (28) yields a -3.2 dB difference, resulting from the compression of the photodiode (This can be viewed as a -1.6 dB correction on I'_{dc}). However, this detector compression is necessary to achieve the desired RF gain. For this received current, the output power of the EDFA was 12 dBm, near its maximum output power of 13 dBm. Because the EDFA was highly compressed, it had a noise figure of 11.3 dB, again necessary to achieve the gain specification. The link output noise was measured on an electrical spectrum analyzer at -148 dBm/Hz, which agrees with (18). Using this value with (12) gives NF_{rf} = 35.5 dB, which agrees with (27) if a +1.6 dB correction is used. The results of the two-tone (2.00 and 2.01 GHz with equal magnitude) SFDR measurement are shown in Fig. 15, resulting in an $OIP3$ = 6.0 dBm. Note that this result agrees with (24) with the -3.2 dB correction. We then use (21) with the measured $OIP3$ and noise floor to calculate SFDR = 102.7 dB·Hz$^{2/3}$. Equivalently, (28) could have been used with the (2/3) × -1.6 dB correction to arrive at SFDR = 102.8 dB·Hz$^{2/3}$. In any case, the link meets the SFDR and RF gain performance requirements with a 35.5 dB RF noise figure. Also note that these parameters can be evaluated at other frequencies by scaling them by the RF gain shown in Fig. 14, the shape of which is due to the frequency response of the MZM and the photodiode.

In summary, this link was designed first by maximizing the optical launch power into the link, limited by the SBS threshold. The EDFA at the output was required to operate in saturation to achieve the desired RF gain, which in turn set the optical noise figure and ultimately the RF noise figure. This design procedure is obviously particular to this link and the accompanying specifications. However, the methodology for other designs should be evident and the necessary equations for such an undertaking have been presented.

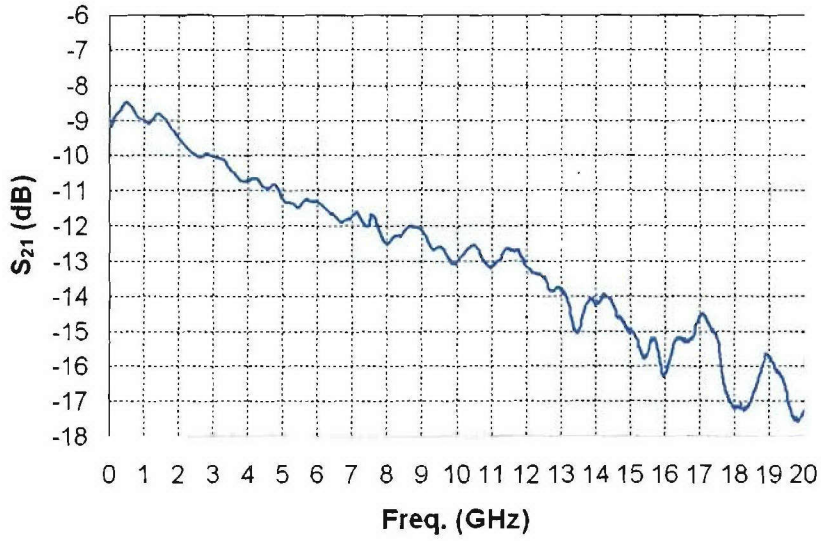

Fig. 14. The RF frequency response for the 20 km link as measured on a network analyzer.

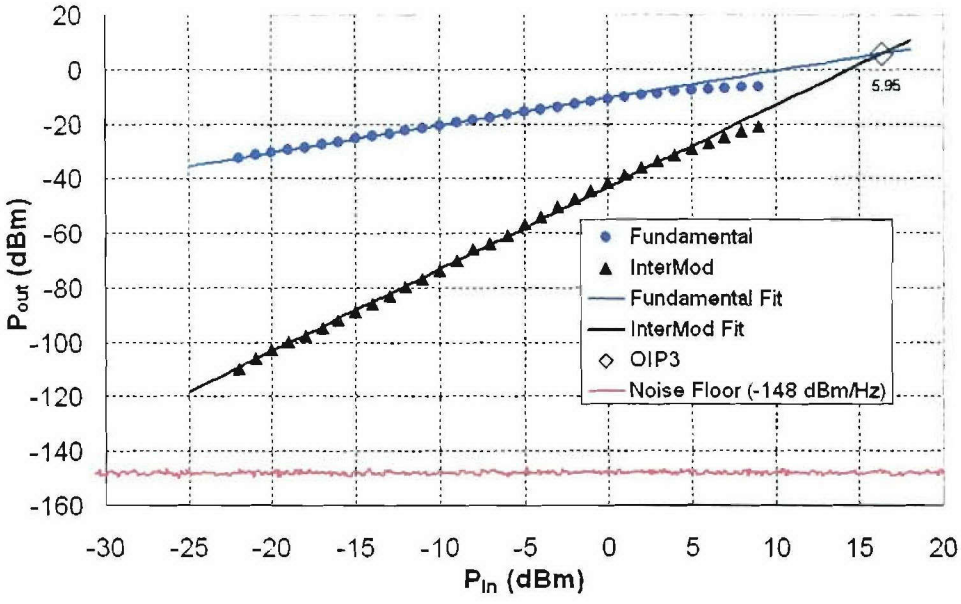

Fig. 15. The results of a two-tone measurement for the 20 km link at 2.00 and 2.01 GHz. Shown are the measured fundamental response, the measured intermodulation response, the extrapolated *OIP*3 and the measured noise floor, resulting in a SFDR of 102.7 $dB \cdot Hz^{2/3}$.

6 CONCLUSIONS

We have presented a self-contained guide for the design and characterization of long-haul analog fiber optic links. We have concentrated on amplitude-modulated single-channel links and considered the metrics of RF gain, RF noise figure, and spurious-free dynamic range. The link design methodology was demonstrated for a 20 km link operating in the signal-spontaneous noise limit, noting that the equations presented can be used for any limiting noise source. Section 2 serves as such a general treatment of analog photonics. The fiber impairments that affect long-haul single-channel transmission were introduced in Section 3, which allows for the signal-spontaneous limited spurious-free dynamic range calculation in Section 4 (again stressing that Sections 2 and 4 can be used together for a general treatment). Section 5 explicitly gives the signal-spontaneous design equations, which were demonstrated for particular link specifications. The equations and methodology, however, can be used in general as guidelines for long-haul link design.

ACKNOWLEDGEMENTS

The authors wish to acknowledge Jennifer Witkowsky, formerly a contractor at NRL, for collecting the data shown in Figs. 6 and 7.

REFERENCES

[1] E. E. Funk, V. J. Urick, S. J. Strutz, J. L. Dexter, and K. J. Williams, "110 km 256-QAM digital microwave over fiber link," in *IEEE MTT-S Digest*, Philadelphia, pp. 269-272, June 2003.

[2] V. J. Urick, J. X. Qiu, F. Bucholtz, C. McDermitt, and K. J. Williams, "4 Gbit/s transmission over single-channel Raman-amplified 105 km link," *Electron. Lett.*, vol. 40, pp. 495-496, Apr. 2004.

[3] E. E. Funk, A. L. Campillo, and D. A. Tulchinsky, "Nonlinear distortion and crosstalk in microwave fiber-radio links," in *IEEE MTT-S Digest*, vol. 3, pp. 1691-1693, June 2002.

[4] A. L. Campillo, F. Bucholtz, J. L. Dexter, and K. J. Williams, "Crosstalk reduction in wavelength division multiplexed analog links through polarization modulation," in *CLEO/IQEC & PhAST Technical Digest*, San Francisco, paper CWQ3, May 2004.

[5] F. Bucholtz, V. J. Urick, and A. L. Campillo, "Comparison of crosstalk for amplitude and phase modulation in an analog fiber-optic link," in *Microwave Photonics Technical Digest*, Ogunquit, pp. 66-69, Oct. 2004.

[6] M. S. Rogge, V. J. Urick, F. Bucholtz, K. J. Williams, and P. Knapp, "Comparison of amplitude and phase modulation crosstalk in hyperfine WDM fiber optic links," in *CLEO/IQEC & PhAST Technical Digest*, Baltimore, May 2005.

[7] V. J. Urick, F. Bucholtz, J. L. Dexter, K. J. Williams, and C. McDermitt, "Increased spurious-free dynamic range for an all-Raman 105 km link using phase modulation and balanced detection," in *CLEO/IQEC & PhAST Technical Digest*, San Francisco, paper CThBB1, May 2004.

[8] V. J. Urick, J. X. Qiu, and F. Bucholtz, "Wide-band QAM-over-fiber using phase modulation and interferometric demodulation," *IEEE Photonics Technol. Lett.*, vol. 16, no. 10, pp. 2374-2376, Oct. 2004.

[9] A. L. Campillo, F. Bucholtz, and K. J. Williams, "Dispersion impairments in analog polarization modulated links," in *Microwave Photonics Technical Digest*, Ogunquit, pp. 104-106, Oct. 2004.

[10] V. J. Urick and F. Bucholtz, "Compensation of arbitrary chromatic dispersion in analog links using a modulation-diversity receiver," *IEEE Photonics Technol. Lett.*, vol. 17, no. 4, pp. 893-895, Apr. 2005.

[11] P. Horowitz and W. Hill, "The Art of Electronics," 2nd ed., New York, Cambridge, pp. 430-431, 1989.

[12] W. V. Sorin, "Noise sources in optical measurements," in *Fiber optic test and measurement*, D. Derickson (editor), Prentice Hall, Upper Saddle River, pp. 597-613, 1998.

[13] K. Y. Lau and A. Yariv, "Ultra-high speed semiconductor lasers," *IEEE Journal of Quantum Electronics*, vol. QE-21, no. 2, pp. 121-138, Feb. 1985.

[14] B. Christensen, J. Mark, G. Jacobsen, and E. Bodtker, "Simple dispersion measurement technique with high resolution," *Electron. Lett.*, vol. 29, no. 1, pp. 132-133, Jan. 1993.

[15] G. P. Agrawal, "Nonlinear fiber optics," 3rd ed., San Diego: Academic Press, 2001.

[16] J. L. Corral, J. Marti, and J. M. Fuster, "General expressions for IM/DD dispersive analog optical links with external modulation or optical up-conversion in a Mach-Zehnder electrooptical modulator," *IEEE Trans. Microwave Theory Tech.*, vol. 49, no. 10, pp. 1968-1976, Oct. 2001.

[17] C. Kittel, "Introduction to solid state physics," 7th ed., New York: Wiley, 1996, pp. 107-111.

[18] J. Zhang and M. R. Phillips, "Modeling intensity noise caused by stimulated Brillouin scattering in optical fibers," in *CLEO Technical Digest*, Baltimore, paper CMH6, May 2005.

[19] G. C. Wilson, T. H. Wood, J. L. Zyskind, J. W. Sulhoff, J. E. Johnson, T. Tanbun-Ek, and P. A. Morton, "SBS and MPI suppression in analogue systems with integrated electroabsorption modulator/DFB laser transmitters," *Electron. Lett.*, vol. 32 no. 16, pp. 1502-1504, Aug. 1996.

[20] N. Yoshizawa and T. Imai, "Stimulated Brillouin scattering suppression by means of applying strain distribution to fiber with cabling," *J. Lightwave Technol.*, vol. 11, pp. 1518-1522, Oct. 1993.
[21] J. Hansryd, F. Dross, M. Westlund, P. A. Andrekson, and S. N. Knudsen, "Increase of the SBS threshold in a short highly nonlinear fiber by applying a temperature distribution," *J. Lightwave Technol.*, vol. 19, no. 11, pp. 1691-1697, Nov. 2001.
[22] X. P. Mao, R. W. Tkach, A. R. Chraplyvy, R. M. Jopson, and R. M. Derosier, "Stimulated Brillouin threshold dependence on fiber type and uniformity," *IEEE Photonics Technol. Lett.*, vol. 4, no. 1, pp. 66-69, Jan. 1992.
[23] C. A. S. de Oliveira, C. K. Jen, A. Shang, and C. Saravanos, "Stimulated Brillouin scattering in cascade fibers of different Brillouin frequency shifts," *J. Opt. Soc. Am. B*, vol. 10, no. 6, pp. 969-972, June 1993.
[24] S. Rae, I. Bennion, and M. J. Cardwell, "New numerical model of stimulated Brillouin scattering in optical fibers with nonuniformity," *Optics Communications*, vol. 123, pp. 611-616, Feb. 1996.
[25] A. Kobyakov, M. Sauer, and J. E. Hurley, "SBS threshold of segmented fibers," in *OFC Technical Digest*, Anaheim, paper OME5, Mar. 2005.
[26] E. Desurvire, "Erbium-doped fiber amplifiers: principles and applications," New York: Wiley, 1994.
[27] P. C. Becker, N. A. Olsson, and J. R. Simpson, "Erbium-doped fiber amplifiers: fundamentals and technology," San Diego: Academic Press, 1999.
[28] M. R. Phillips and T. E. Darcie, "Lightwave analog video transmission," in *Optical Fiber Telecommunications IIIA*, San Diego: Academic, 1997.
[29] S. A. Maas, "Nonlinear microwave and RF circuits," Boston, Artech House: 2003.
[30] P. Hernday, "Dispersion measurements," in *Fiber Optic Test and Measurement*, Upper Saddle River, Prentice Hall: 1998.